

SCIENTIFIC REPORTS



OPEN

High Performance All-solid Supercapacitors Based on the Network of Ultralong Manganese dioxide/Polyaniline Coaxial Nanowires

Junli Zhou^{1,3}, Lin Yu¹, Wei Liu³, Xiaodan Zhang², Wei Mu³, Xu Du³, Zhe Zhang³ & Yulin Deng³

In recent years, thin, lightweight and flexible solid supercapacitors are of considerable interest as energy storage devices. Here we demonstrated all-solid supercapacitors (SSCs) with high electrochemical properties, low self-discharge characteristics based on manganese dioxide/polyaniline (MNW/PANI) coaxial nanowire networks. The synergistic effect of MnO₂/PANI plus the unique coaxial nanostructure of the ultralong nanowires with a highly interconnected network effectively enhance the conductivity and capacitive performance of the SSCs device. The MNW/PANI composite with 62.5% MnO₂ exhibits an outstanding areal specific capacitance reaching 346 mF/cm² at 5 mV s⁻¹ which is significant higher than most previously reported solid supercapacitors (15.3 mF/cm²–109 mF/cm²) and is close to the that of the best graphene films solid state supercapacitors (372 mF/cm²). In contrast, only 190 mF/cm² of areal specific capacitance was obtained for the pure MnO₂ NW network. The supercapacitors also exhibited low leakage current as small as 20.1 μA, which demonstrated that the MNW/PANI SSCs have great potential for practical applications.

The design and synthesis of nanostructure materials have attracted much attention because of their novel properties and potential applications in catalyst, environment protection, sensors, and energy storage devices. Nowadays, various nanostructure materials have been synthesized by various strategies, such as peptide-directed simultaneous, layer-by-layer (LbL) assembly technique and biomineralization etc^{1,2}. However, it still remains a great challenge to develop facile and economic synthetic methods for the construction of hierarchical architectures with novel tunable material properties.

Energy storage devices, such as Li-ion batteries, fuel cells and supercapacitors, are considered as an important part of the clean energy. Among the existing energy storage devices, much effort has been devoted to lightweight and flexible supercapacitors due to their fast charge and discharge ability, high power density and long life cycles^{3–6}. Up to now, many supercapacitor materials focused on different carbon-based nanomaterials, such as graphene^{7,8}, carbon cloth⁹, carbon nanotube (CNTs)¹⁰, etc. Moreover, surface modification of carbon based materials using pseudocapacitor materials such as conducting polymer and metal oxides can effectively enhance their electrochemical performance^{11,12}. Especially, the graphitic carbons after chemical modification/doping have novel tunable properties, including the controllability of electronic energy level, charge density, surface energy and surface reactivity, which benefit for flexible electronics/optoelectronics, energy conversion/storage. However, the inert chemical structures with low surface energy for CNTs and graphene are the principal bottleneck for cost-effective solution processing¹³.

Pseudocapacitive-type electrode materials such as transition metal oxides and conductive polymers have attracted much attention due to their low cost but high electrochemical performance. Transition metal oxides

¹Faculty of Chemical Engineering and Light Industry, Guangdong University of Technology, Guangzhou 510006, Guangdong, China. ²School of Materials Science & Engineering, Georgia Institute of Technology, Atlanta, GA 30332, USA. ³School of Chemical & Biomolecular Engineering, Georgia Institute of Technology, Atlanta, GA 30332, USA. Correspondence and requests for materials should be addressed to L.Y. (email: gych@gdut.edu.cn) or Y.D. (email: yulin.deng@ipst.gatech.edu)

and conducting polymers such as manganese dioxides (MnO_2) and polyaniline (PANI) have been found to exhibit excellent pseudocapacitive behavior^{14–17}. Among the transition metal oxides, manganese dioxide (MnO_2) with different morphologies has been considered as an alternative electrode material due to the low cost, high theoretical specific capacitance (1370 F g^{-1}) and environmental friendly energy conversion^{18,19}. Unfortunately, the poor electronic conductivity of MnO_2 (10^{-5} to $10^{-6} \text{ S cm}^{-1}$)²⁰ may cause the decrease in the specific capacitance and power density of supercapacitors during high-rate charge-discharge process. In order to improve the electrochemical performance of MnO_2 , much effort has been made to fabricate composite materials with good electrical conductivity materials even high cost noble metals^{21,22}. Conducting polymers, such as PANI has been extensively studied as electrode materials because of their ease of synthesis, good electrical conductivity, high chemical stability, high doping properties and low cost. Heterostructured nanomaterials have been attracted particular attention because the synergic properties and functionalities of these combined materials enable this composite material to exhibit a high electrochemical performance. Sumboja *et al.* have prepared manganese dioxide/polyaniline coaxial nanowires by self-terminated double surfactant polymerization for pseudocapacitor electrode, showing specific capacitance of 498 F g^{-1} in Na_2SO_4 electrolyte²³. Jaidev *et al.* reported a novel binary hybrid nanocomposite based on polyaniline (PANI) and α - MnO_2 nanotubes (MNTs) and found that the nanocomposite exhibited good electrochemical performance with a specific capacitance of 626 F g^{-1} in H_2SO_4 electrolyte²⁴. Although high performance MnO_2 based supercapacitors have attracted much attention due to their higher power density, longer life cycles, faster charge and discharge rate than batteries^{25–27}, almost all PANI- MnO_2 based supercapacitors used electrolyte solution as the charge transfer medium^{28–30}. In particular, solid and lightweight supercapacitors have been a new focus of researches^{31–33}. Considering the safety issues, the SSCs are superior to the traditional liquid electrolyte supercapacitors, since the liquid electrolyte leakage is a severe issue, especially when the materials are hazardous for human and environment. In this context, a simple and low-cost method to fabricate light weight solid supercapacitors is greatly desired for energy storage devices.

Here we demonstrated the solid state supercapacitors (SSCs) with high electrochemical properties, low self-discharge characteristics and high stability based on manganese dioxide/polyaniline (MNW/PANI) coaxial nanowire networks. Practically, instead of the conventional hydrothermal method using Mn^{II} (MnSO_4) and oxidizing agent (KMnO_4 , NaClO_3)^{34,35}, in this work, MnO_2 nanosheet-assisted hydrothermal and *in situ* polymerization method was designed to construct the well dispersed MNW/PANI coaxial configuration. Such nanostructured MNW/PANI coaxial configuration with highly interconnected network provides an excellent structure for supercapacitor electrodes, which is favorable for fabricating a high efficient supercapacitor. Besides, a novel and simple method using the polyvinyl alcohol (PVA)/ H_3PO_4 electrolyte to fabricate the MNW/PANI based SSCs is presented. The fabricated SSCs exhibited high electrochemical performance, which is significantly higher than most flexible supercapacitors reported in literature. And a practical use of the SSCs devices to light up the LEDs demonstrated the great potential in energy storage devices.

Results and Discussion

The ultralong MnO_2 NW were prepared first via one-pot reactions of MnO_2 nanosheets and KClO_3 at 160°C for 12 h (Supporting Information Experimental Section). MnO_2 nanosheets were prepared using the same method as previously reported³⁶. As shown in Fig. 1a, the Birnesstie type δ - MnO_2 showed two diffraction peaks which could be indexed as (001) and (002), respectively. After the ultrasonic treatment with TMAOH, the absence of reflections peaks indicated the loss of the original crystalline structure, suggesting that the Birnesstie type δ - MnO_2 was delaminated to the individual nanosheets³⁷. TEM image showed that the nanosheets are extremely thin, which looks like graphene (Fig. 1b). It was interesting to find that these thing δ - MnO_2 nanosheets could be further converted to α - MnO_2 ultralong nanowires. The XRD results of α - MnO_2 NW are shown in Fig. 1c, exhibiting pure tetragonal phase (space group $I4/m$) of α - MnO_2 with lattice constants of $a = 9.7847 \text{ \AA}$, $b = 9.7847 \text{ \AA}$ and $c = 2.8630 \text{ \AA}$ (JCPDS No.44-0141). The morphological evolution of Two-Dimensional (2D) MnO_2 nanosheets and their shape transformation to One-Dimensional (1D) ultralong MnO_2 NW was investigated by time-dependent SEM images, as shown in Fig. 2. At the initial stage, δ - MnO_2 nanosheets were observed and they were gradually changed into 1D nanowire morphology with the progress of reaction time. Li *et al.* have reported the rolling growth mechanism for δ - MnO_2 nanosheets to form the α - MnO_2 NW³⁸. However, in our study, no curling or rolling of the nanosheets was observed (Fig. 2b). Although the actual mechanism of conversion of δ - MnO_2 nanosheets to α - MnO_2 NW in our experiment is not clear, it is believed that the process obeys a recrystallization process which may be similar to the previous report³⁹. In the recrystallization process, the new α - MnO_2 nuclei were first formed in the solution. The δ - MnO_2 nanosheets dissolve and recrystallized as 1D nanowires. The diameter and length of the nanowires increase with time and finally form the ultralong nanowire networks (Fig. 2c).

The PANI/ MnO_2 coaxial nanowires were then obtained by using the α - MnO_2 NW as the oxidant template to initiate the polymerization of aniline in H_2SO_4 solution (Supporting Information Experimental Section). A series of time-dependent experiments was conducted. The XRD patterns for MNW/PANI still exhibited α - MnO_2 phase with reduced intensity of MnO_2 characteristic peaks for 8 h. The reduced diffraction intensity is because that the PANI layer can cause the X-ray scattering. After the extension of the reaction time to 14 hours, α - MnO_2 as oxidant and template was almost removed. No α - MnO_2 peaks were observed (Fig. 1c). Two peaks at 2θ 20° and 25° shown in Fig. 1c represent the periodicities parallel (100) and perpendicular (110) to the PANI chain respectively⁴⁰. PANI coating on MnO_2 NW was also successfully confirmed by thermogravimetric (TG) measurements (Fig. 1d). For comparison, we have also prepared MnO_2 NW and PANI powder. From the TG curves, it can be inferred that the mass of MnO_2 in the composite MNW/PANI (8h) and MNW/PANI (14h) is about 81% and 62.5%, respectively.

The ultralong MnO_2 nanowires are shown in Fig. 3a. The actual length of the MnO_2 NW is too long to be measured from SEM image. The SEM and TEM images (Fig. 3a,c) indicate that the diameter of the MnO_2 NW is about 50 nm. The α - MnO_2 NW free-standing membrane with a good mechanical stability could be prepared by simply filtering the NW suspension on a filter paper (Figure S1). The nanowires are physically entangled and interconnected

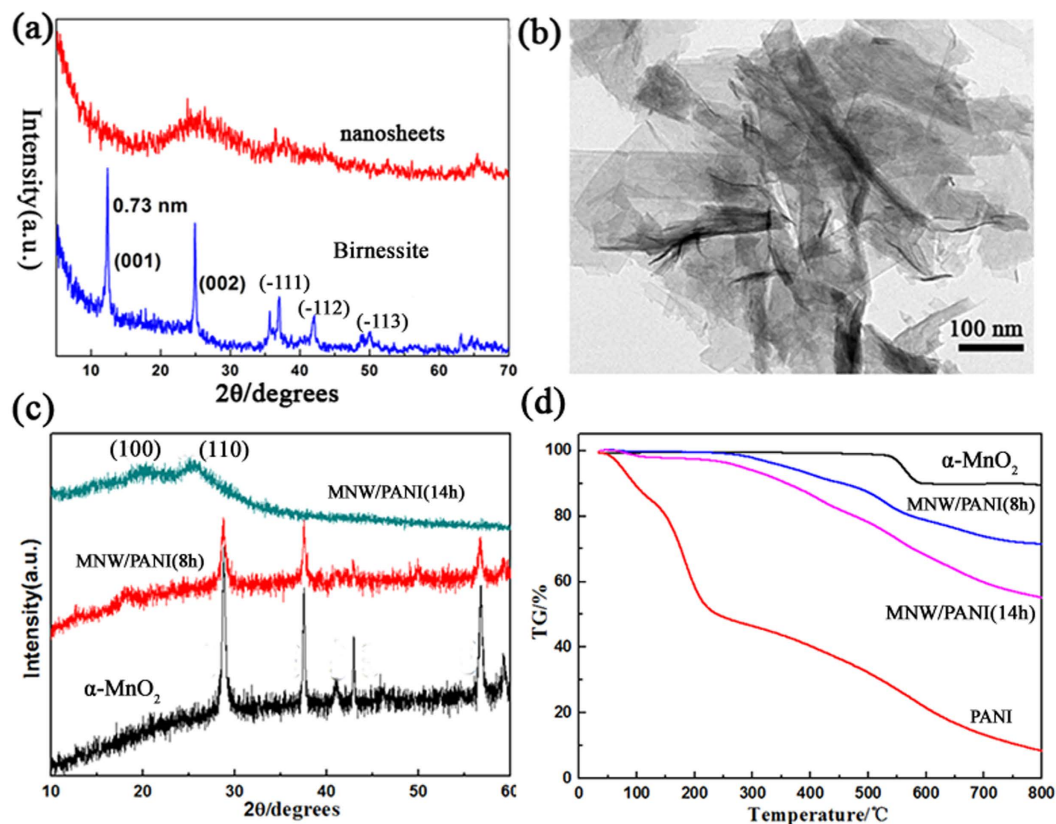


Figure 1. (a) XRD patterns for Birnessite type MnO_2 and nanosheets. (b) TEM image for MnO_2 nanosheets. (c) XRD patterns and (d) TGA curves for $\alpha\text{-MnO}_2$ nanowires, PANI, MNW/PANI(8h), MNW/PANI(14h).

in the porous network membrane. Because $\alpha\text{-MnO}_2$ NW is an oxidation agent that can initiate the polymerization of aniline, when it was immersed into aniline solution, polymerization started on the surface of MnO_2 NWs. If the concentration of aniline monomer in the solution is low, a uniform and thin PANI coating layer on $\alpha\text{-MnO}_2$ NW was obtained. As the reactions proceeded, PANI shells grew and $\alpha\text{-MnO}_2$ NW was partially reduced spontaneously. Then the well-dispersed MNW/PANI with uniform interconnection networks was obtained. The networks possess a continuously cross-linked structure with pore sizes in the range of sub-micrometer to several micrometers (Fig. 3b). Such network structure will be beneficial for filtrating solid electrolyte that can transport electrons between two MnO_2 /PANI electrodes in a supercapacitor. Uniform coating of PANI has been observed on MnO_2 NW, demonstrating the formation of MNW/PANI coaxial nanowires (Fig. 3d). Successful PANI coating on MnO_2 NW surface is also confirmed by FTIR (Figure S2 in supporting information). The bands around 523 and 465 cm^{-1} in both spectrums can be assigned to the Mn–O stretching vibration. Bands at 1569 and 1482 cm^{-1} in MNW/PANI coaxial NW is due to the stretching vibration of quinoid and benzenoid ring, indicating that the resultant PANI was in its emeraldine state²³. The peak around 1292 cm^{-1} is corresponding to C–NH⁺ stretching (characteristic of the polaron form of PANI emeraldine salt) and the strong peak around 1132 cm^{-1} is the characteristic peak of PANI conductivity²⁴. FTIR spectrum of the MNW/PANI coaxial NW shows characteristic bands of PANI as well as of MnO_2 , which confirms the presence of both components in the coaxial heterostructures.

The designed MNW/PANI interconnection porous networks combined the advantages of high theoretical specific capacitance of $\alpha\text{-MnO}_2$ NW and the good electrical conductivity of PANI. To evaluate the electrochemical activity of MNW/PANI materials, solid supercapacitor devices were assembled using MNW/PANI as the working electrodes and PVA/ H_3PO_4 as solid electrolyte. The working electrodes were fabricated by compressing a mixture of the MNW/PANI-acetylene black- polytetrafluoroethylene (PTFE) with a weight ratio of 0.85:0.15:0 on Ni foam at 0.2 MPa. The dimension of the electrode is $1\text{ cm} \times 1\text{ cm}$. Two symmetric pieces of identical MNW/PANI electrodes and a separator (filter paper, Whatman Corporation) were immersed into the electrolyte (PVA/ H_3PO_4) for 10 min, and then taken out to fabricate as a sandwich type of supercapacitor (Figure S3). Ni foam was used as both a current collector and a mechanical support due to the high conductivity and the instinct macroporous structure to hold the electrode materials^{41–43}.

Cyclic voltammetry (CV) measurements were performed to test the electrochemical properties of the designed MNW/PANI networks as electrode materials using a three-electrode cell. Figure 4a shows that the CVs for MNW/PANI (8h) over a range of scan rates of 2, 5, 10 mV/s, with a potential window of -0.4 – 0.6 V versus a saturated calomel electrode (SCE). The CV curves at low scan rate show a nearly rectangular shape, indicating good electrochemical capacitive behavior of the SSCs. Although the CV curves were somewhat distorted when the scan rate increases up to 10 mV/s, the SSCs still exhibited good electrochemical capacitance performance. The areal

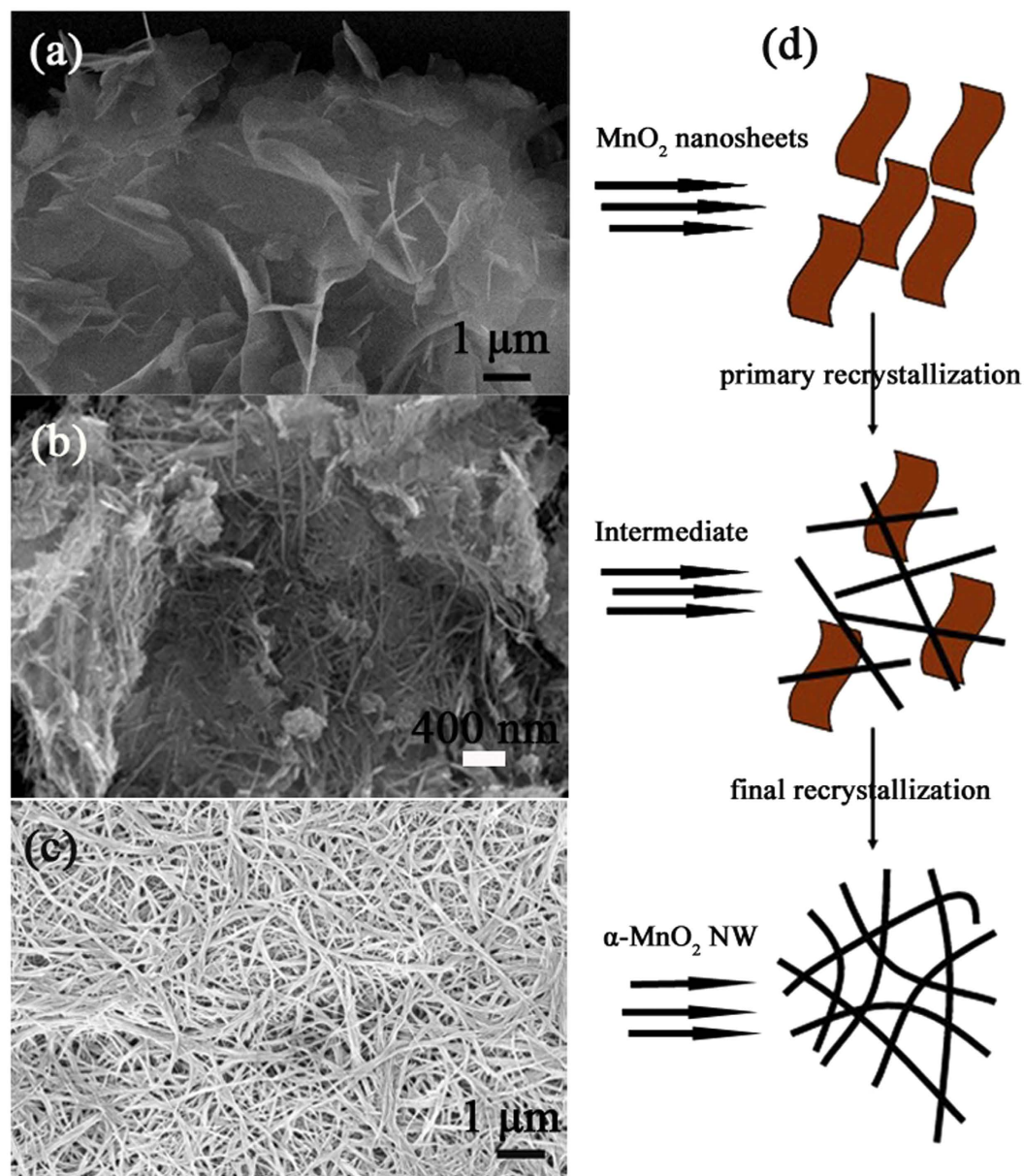


Figure 2. Schematic illustration of the formation from 2D Nanosheet to 1D Nanowires.

capacitances can be calculated from the CV curves according to $C_s = I / (2 \cdot s \cdot \nu)$, where s is the area of one electrode sheet, ν is the potential sweep rate, and I is the applied current defined by $I = A / \Delta V$, where A presents the integrating area of the curves and ΔV is the voltage difference. The areal capacitances calculated from the CV profiles decreased from 293 to 157 mF/cm² with the scan rate rise from 2 to 10 mV/s. The decrease of capacitance is mainly because that the redox reactions of insertion-deinsertion of electrolyte are a time-dependent process^{44,45}.

Galvanostatic charging/discharging tests were conducted under a stable potential window of 0–1.0 V at different current densities of 0.5, 1.5 and 2.5 mA/cm², and the results are shown in Fig. 4b. It was observed that the discharge curves at 0.5 mA/cm² show two plateaus at about 0.7 V and 0.3 V, respectively. The higher one is due to oxidation of Emeraldine Salt (ES) to pernigraniline, and the lower one is further oxidation of Mn(III) to Mn(IV). Moreover, the discharge profiles of the electrodes are not standard straight lines, but somewhat curved in nature, exhibiting a pseudocapacitive characteristic. The areal capacitance of MNW/PANI supercapacitors with different PANI deposition time and different scan rates are given in Fig. 4c. For comparison, the C_s for the bare ultralong α -MnO₂ NW was also tested and calculated to be 263 mF/cm² at 2 mV/s. The good capacitive behavior of MnO₂ is due to the fast and reversible surface redox reactions of MnO₂⁴⁶. The C_s improves significantly after coating a layer of PANI. The calculated C_s of MNW/PANI (14h) at 2 mV/s (485 mF/cm²) is much higher than pure α -MnO₂ NW (263 mF/cm²) and pure PANI (39.75 mF/cm²) which indicates the coordinated contribution of the pseudocapacitance effect of PANI coated on the MnO₂ NW. Moreover, the C_s for MNW/PANI increases with the increase of deposition time due to the increasing amounts of PANI. Meanwhile the C_s also increases with the decrease of scan

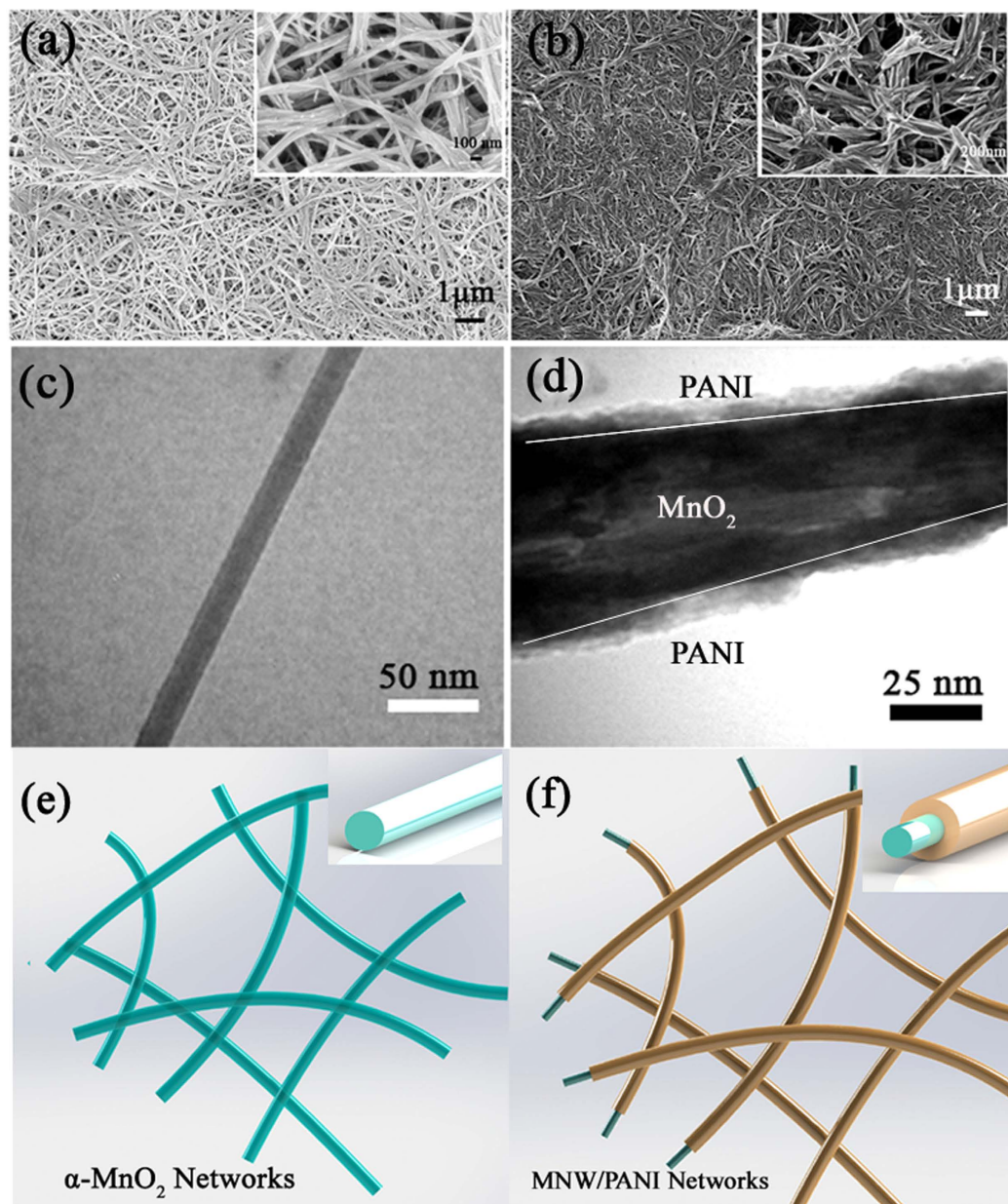


Figure 3. SEM images of (a) α -MnO₂, (b) MNW/PANI (8 h). TEM images of (c) α -MnO₂ NW, (d) MNW/PANI (8 h). (e) Schematics of *In situ* polymerization of aniline based α -MnO₂ NW.

rates due to more adequate Faradaic reactions at lower scan rates⁴⁷. The C_s for MNW/PANI (14 h) supercapacitors was calculated to be 346 mF/cm² at the scan rate of 5 mV/s, which is significant higher than most previously reported solid supercapacitors (15.3 mF/cm²–109 mF/cm²)^{32,48–51} and is close to that of the best graphene films solid state supercapacitors (372 mF/cm²)⁷. The enhanced capacitance for MNW/PANI in this work can be attributed to several reasons. Firstly, the well dispersed nature and the highly mesoporous structure of the designed MNW/PANI interconnection networks, which facilitates more ions transfer to the porous structure having more redox reactions. As shown in Figure S4 and Table1 (Supporting information), the specific surface area of MNW/PANI (105 m² g⁻¹) is lower than MnO₂ NW (163 m² g⁻¹). However, it is interesting that the MNW/PANI has larger pore volume 0.71 cm³ g⁻¹ with large average pore diameter (23.45 nm). Enhancement of internal pore volume may therefore be responsible for increasing the capacitance, which enhances more accessibility to the electrolyte for internal surface adsorption in the electrode. Secondly, after coating a thin layer of PANI, the electric resistance within MnO₂ NW networks is reduced. The Electrochemical Impedance Spectroscopy (EIS) measurement results are shown in Fig. 4d and the equivalent circuit is present in Figure S5. The equivalent circuit includes the following parameters: equivalent series resistance (Rs), charge-transfer resistance (Rct), double layer capacitance (CDL), pseudocapacitance (Cps) and Warburg behaviour (W). At high frequency range, the value of the intercept at the real axis is used to estimate the equivalent series resistance (Rs) including electrolyte resistance, electrode resistance

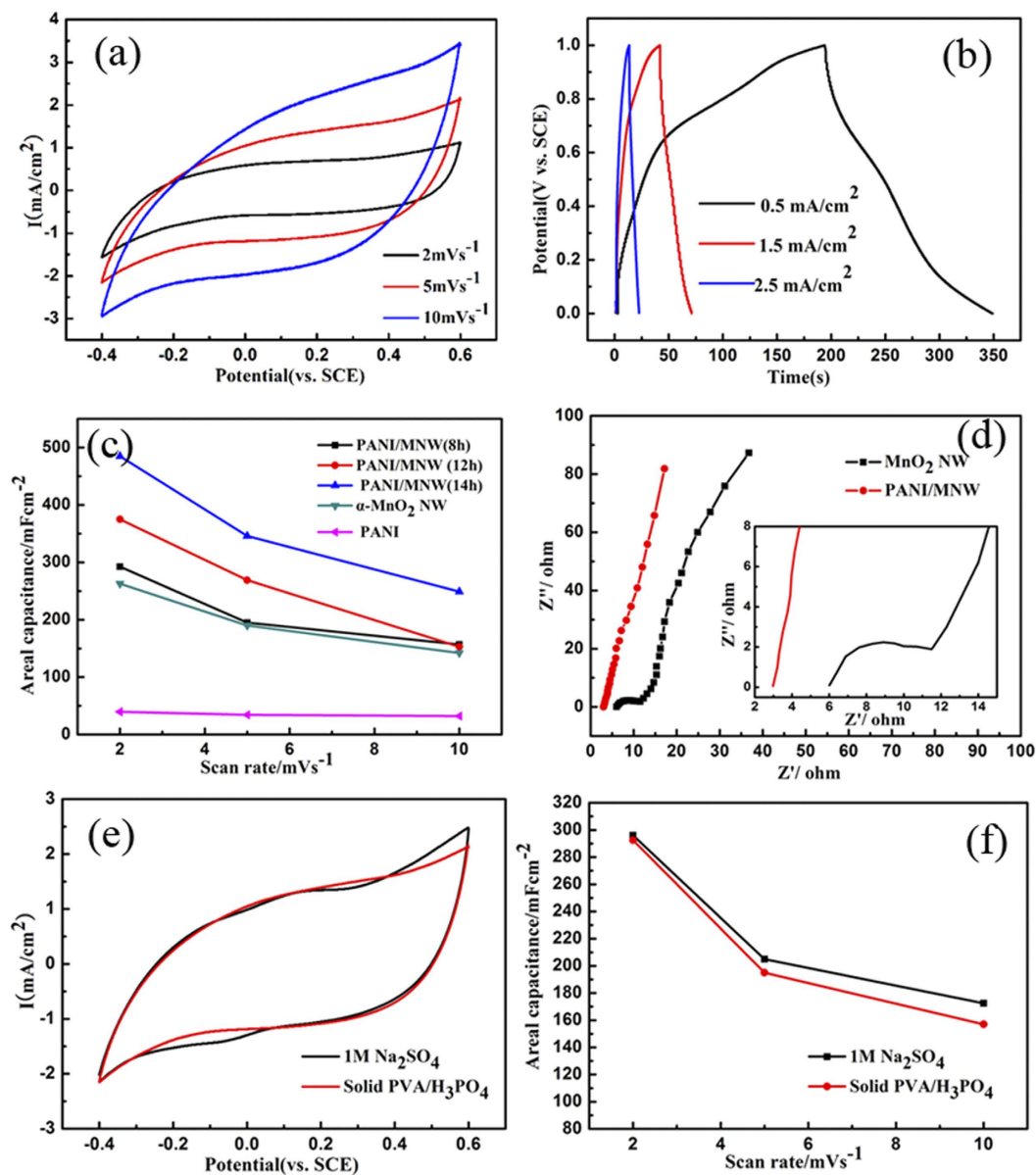


Figure 4. (a) Cyclic voltammograms (CV) and (b) galvanostatic charge/discharge curves of solid supercapacitor for MNW/PANI (8h). (c) Specific areal capacitance C_s vs scan rates for different PANI deposition time, ranging from 8 to 14 h. (d) Nyquist plots of MNW/PANI and MnO_2 NW. (e) CV at a scan rate of 5 mV s^{-1} and (f) Specific areal capacitance C_s vs scan rates curves of MNW/PANI (8 h) in $1 \text{ M Na}_2\text{SO}_4$ solution and in PVA/ H_3PO_4 solid electrolyte.

and the contact resistance between the electrode and electrolyte. The R_s value reduced from 6 to 2.9Ω compared MnO_2 NW with MnO_2 NW which indicates the uniform PANI coating is electrostatically bonded to the MnO_2 NW²³. The formation of mesoporous structure for MNW/PANI in the designed synthesis method is responsible for lower R_s value. The low R_s of the samples help to guarantee the high capacitance. Moreover, no distinct semicircle was observed for the plot of MNW/PANI compared to MnO_2 NW, which indicates that the MNW/PANI coaxial configuration resulted in the lower charge transfer resistance (R_{ct}) between the active material interface and electrolyte. In addition, Nyquist plot of MNW/PANI SSCs shows a straight line in the low frequency region which is attributable to Warburg impedance (W). The angle between the linear region of the plots and the real axis (Warburg region) resulted from the frequency dependence of ion diffusion and transport in the electrolyte. The angle goes larger after coating PANI which indicates the short ion diffusion path in the electrolyte to the electrode interface (Figure S6). Finally, good coordination between PANI shell and MnO_2 NW core help to improve the capacitance of MNW/PANI SSCs. PANI shell could be well electrostatically bonded in the MnO_2 NW interface through *in situ* polymerization using ultralong MnO_2 NW as oxidant template. As proved in CV curves previously, the C_s for MNW/PANI is 1.8 times of pure MnO_2 NW and 12 times of pure PANI which is not the simple additive effect of PANI and MnO_2 . The comparisons of the as fabricated MNW/PANI supercapacitors in $1 \text{ M H}_2\text{SO}_4$ solution

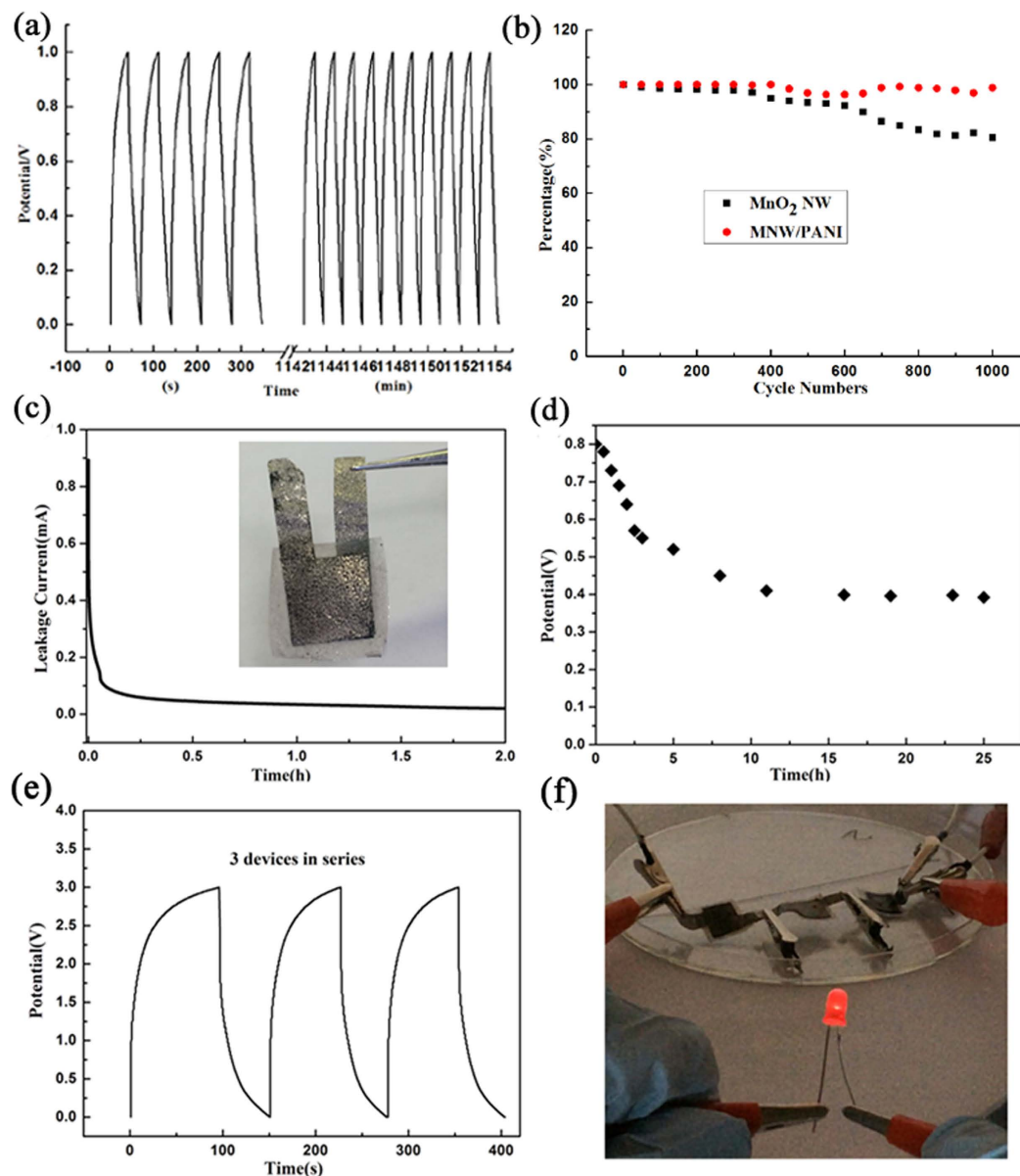


Figure 5. (a) Charge/discharge curves of the MNW/PANI device at the current density of 1.5 mA/cm^2 and (b) Cyclic stability for MNW/PANI and MnO_2 NW device. (c) Leakage current curves of the solid device charged at 2 mA to 0.8 V and kept at 0.8 V for 2 h (inset: photographs of the symmetric supercapacitor based on MNW/PANI). (d) Self discharge curve of the device after charging at 0.8 V for 15 min . (e) Galvanostatic charge/discharge curves at 1.5 mA of the three SSCs connected in series. (f) A LED lighted by a device composed of three SSCs connected in series.

and in $\text{PVA/H}_3\text{PO}_4$ solid electrolyte are shown in CV curves at a scan rate of 5 mV/s (Fig. 4e). The two curves show the same patterns with slightly difference. The areal capacitance of 195 mF/cm^2 at a scan rate of 5 mV/s is very close to the supercapacitor measured at $1 \text{ M H}_2\text{SO}_4$ electrolyte (205 mF/cm^2). The nearly overlapped CV curves indicate that the electrochemical properties of MNW/PANI supercapacitors in $\text{PVA/H}_3\text{PO}_4$ solid electrolyte are almost as good as they are in H_2SO_4 aqueous solution (Fig. 4f), which suggests the fast ion transportation of $\text{PVA/H}_3\text{PO}_4$ solid electrolyte^{7,33}.

The electrochemical stability of the SSCs device was examined under continuous charge/discharge test at the current density of 1.5 mA/cm^2 for $1,000$ cycles (Fig. 5a). The MNW/PANI SSCs device almost kept the same performance in the first 400 cycles test and a slightly fluctuation with 1.5% degradation of the specific capacitance all the way to $1,000$ cycles, indicating good stability of the MNW/PANI sample (Fig. 5b). However, the specific capacitance for pure MnO_2 NW faded significantly with 18% degradation at the end of cycles, which is attributed to the dissolution of MnO_2 into the electrolyte. Coating a thin layer of PANI on MnO_2 was observed to improve the long term cycling stability of MnO_2 . For practical application, it is very important to evaluate the self-discharge characteristics and leakage current of the solid supercapacitors which are few discussed in recent reports^{7,50}. For

the leakage current test, the solid device (inset picture in Fig. 5c) was first charged to 0.8 V at 2 mA and kept at 0.8 V for 2 h to acquire the current data. As shown in Fig. 4c, the leakage current decreased significantly in the first 10 min (from 0.9 mA to 57.8 μ A) and quickly stabilized at 20.1 μ A, which is essentially the leakage current through the device. This value is comparable to that of polyaniline/carbon nanotube composite supercapacitor (17.2 μ A)¹², indicating the very small leakage current of the designed SSCs device. The stability of the solid supercapacitors is demonstrated by a self-discharge test represented by the open-circuit voltage versus time course. As shown in Fig. 5d, the solid supercapacitors after being charged at 0.8 V for 15 min underwent a rapid self-discharge process within several minutes and reached a stable output voltage at 0.42 V after 25 h. The result is comparable to previous results of solid supercapacitors (0.3–0.4 V)^{7,52}. These results demonstrate that the solid supercapacitors in our studies exhibit excellent low self-discharge characteristics, which is a big concern for practical applications in electronics. As shown in Fig. 5f, three SSCs were connected in series to light a light-emitting diode (LED), the lowest working potential is 1.6 V. Every SSCs used here has the same area (1 cm²) and mass loading (~8.5 mg for each electrode). The whole series device was evaluated by galvanostatic charge/discharge measurements (Fig. 5e). The potential window extended from 1.0 V for single SSCs to 3.0 V for the series device. After charged at 3 V for 15 s, the series device could light the LED for about 90 s (Fig. 5f and see supporting information, video 1). Electrochemical energy storage is associated with electron transfer. The EIS measurement results indicated that the lower ESR and charge transfer resistance could improve a series of fast, reversible electron-transfer reactions (Figure S7).

In summary, MnO₂ nanosheet-assisted hydrothermal and *in situ* polymerization method was designed to construct the well dispersed MNW/PANI coaxial configuration. We have successfully fabricated MNW/PANI SSCs with high electrochemical performance. The well dispersed and highly mesoporous of MNW/PANI interconnection networks provided good structure for supercapacitors electrode, and the good interaction between PANI and MnO₂ NW provided fast electron and charge transportation paths to achieve high capacitance. Higher C_c was achieved for MNW/PANI(14 h) reaching 346 mF/cm² at 5 mV s⁻¹ as compared to the pristine MnO₂ NW(190 mF/cm²). The self-discharge characteristics and practical use as power source for LED lighting indicated the great potential application in electronics.

References

- Chen, C.-L. & Rosi, N. L. Peptide-Based Methods for the Preparation of Nanostructured Inorganic Materials. *Angew. Chem. -Int. Edit.* **49**, 1924–1942 (2010).
- Ariga, K. *et al.* Layer-by-layer Nanoarchitectonics: Invention, Innovation, and Evolution. *Chem. Lett.* **43**, 36–68 (2014).
- Huang, H.-S. *et al.* Evaporation-Induced Coating of Hydrated Ruthenium Oxide on Mesoporous Silica Nanoparticles to Develop High-Performance Supercapacitors. *Small* **9**, 2520–2526 (2013).
- Shao, M. *et al.* Supercapacitors: Hierarchical Conducting Polymer@Clay Core-Shell Arrays for Flexible All-Solid-State Supercapacitor Devices. *Small* **11**, 3529–3529 (2015).
- Bastakoti, B. P. *et al.* Mesoporous Carbon Incorporated with In₂O₃ Nanoparticles as High-Performance Supercapacitors. *Eur. J. Inorg. Chem.* **2013**, 1109–1112 (2013).
- Dai, S. *et al.* MnO₂@KCu₂S₄ NWs hybrid compositions for high-power all-solid-state supercapacitor. *J Power Sources* **274**, 477–482 (2015).
- Xu, Y. *et al.* Flexible Solid-State Supercapacitors Based on Three-Dimensional Graphene Hydrogel Films. *ACS Nano* **7**, 4042–4049 (2013).
- Salunkhe, R. R., Hsu, S.-H., Wu, K. C. W. & Yamauchi, Y. Large-Scale Synthesis of Reduced Graphene Oxides with Uniformly Coated Polyaniline for Supercapacitor Applications. *Chem Sus Chem* **7**, 1551–1556 (2014).
- Guo, D. *et al.* High performance NiMoO₄ nanowires supported on carbon cloth as advanced electrodes for symmetric supercapacitors. *Nano Energy* **8**, 174–182 (2014).
- Kang, Y. J. *et al.* All-Solid-State Flexible Supercapacitors Fabricated with Bacterial Nanocellulose Papers, Carbon Nanotubes, and Triblock-Copolymer Ion Gels. *ACS Nano* **6**, 6400–6406 (2012).
- Tao, J. *et al.* Solid-State High Performance Flexible Supercapacitors Based on Polypyrrole-MnO₂-Carbon Fiber Hybrid Structure. *Sci. Rep.* **3**, 2286 (2013).
- Meng, C. *et al.* Highly Flexible and All-Solid-State Paperlike Polymer Supercapacitors. *Nano letters* **10**, 4025–4031 (2010).
- Maiti, U. N. *et al.* Carbon: 25th Anniversary Article: Chemically Modified/Doped Carbon Nanotubes & Graphene for Optimized Nanostructures & Nanodevices (Adv. Mater. 1/2014). *Adv Mater* **26**, 2–2 (2014).
- Ding, Y. L. *et al.* Coaxial MnO/C nanotubes as anodes for lithium-ion batteries. *Electrochim Acta* **56**, 5844–5848 (2011).
- Chen, W. *et al.* Alshareef, H. N. High-performance nanostructured supercapacitors on a sponge. *Nano letters* **11**, 5165–5172 (2011).
- Meng, Y., Wang, K., Zhang, Y. & Wei, Z. Hierarchical porous graphene/polyaniline composite film with superior rate performance for flexible supercapacitors. *Adv Mater* **25**, 6985–6990 (2013).
- Shi, Y. *et al.* Nanostructured conductive polypyrrole hydrogels as high-performance, flexible supercapacitor electrodes. *J. Mater. Chem. A* **2**, 6086–6091 (2014).
- Hu, X. *et al.* Chen, J. ϵ -MnO₂ nanostructures directly grown on Ni foam: a cathode catalyst for rechargeable LiO₂ batteries. *Nanoscale* **6**, 3522 (2014).
- Wang, S. *et al.* Peanut-like MnO@C core-shell composites as anode electrodes for high-performance lithium ion batteries. *Nanoscale* **6**, 3508–3512 (2014).
- Qiu, Y. *et al.* Electrodeposition of manganese dioxide film on activated carbon paper and its application in supercapacitors with high rate capability. *RSC Advances* **4**, 64187–64192 (2014).
- Han, Q. *et al.* Enhanced hydrogen peroxide sensing by incorporating manganese dioxide nanowire with silver nanoparticles. *Electrochem Commun* **38**, 110–113 (2014).
- Dai, Y., Tang, S., Vongehr, S. & Meng, X. Silver Nanoparticle-Induced Growth of Nanowire-Covered Porous MnO₂ Spheres with Superior Supercapacitance. *ACS Sustain. Chem. Eng.* **2**, 692–698 (2014).
- Sumboja, A. *et al.* Significant electrochemical stability of manganese dioxide/polyaniline coaxial nanowires by self-terminated double surfactant polymerization for pseudocapacitor electrode. *J Mater Chem* **22**, 23921 (2012).
- Jaidev, Jafri, R. I., Mishra, A. K. & Ramaprabhu, S. Polyaniline-MnO₂nanotube hybrid nanocomposite as supercapacitor electrode material in acidic electrolyte. *J Mater Chem* **21**, 17601–17605 (2011).
- Miller, J. R. & Simon, P. Electrochemical Capacitors for Energy Management. *Science* **321**, 651–652 (2008).
- Yu, Z., Tetard, L., Zhai, L. & Thomas, J. Supercapacitor electrode materials: nanostructures from 0 to 3 dimensions. *Energy & Environmental Science*, **8**, 702–730 (2015).
- Shivakumara, S., Kishore, B., Penki, T. R. & Munichandraiah, N. Symmetric supercapacitor based on partially exfoliated and reduced graphite oxide in neutral aqueous electrolyte. *Solid State Commun* **199**, 26–32 (2014).

28. Zhou, Z., Cai, N. & Zhou, Y. Capacitive characteristics of manganese oxides and polyaniline composite thin film deposited on porous carbon. *Mater Chem Phys* **94**, 371–375 (2005).
29. Sun, L.-J. *et al.* Electrodeposited hybrid films of polyaniline and manganese oxide in nanofibrous structures for electrochemical supercapacitor. *Electrochim Acta* **53**, 3036–3042 (2008).
30. Chen, L. *et al.* Synthesis and electrochemical performance of polyaniline–MnO₂ nanowire composites for supercapacitors. *J Phys Chem Solids* **74**, 360–365 (2013).
31. Zhang, X. *et al.* Solid-state, flexible, high strength paper-based supercapacitors. *J. Mater. Chem.A* **1**, 5835 (2013).
32. Yuan, L. *et al.* Flexible Solid-State Supercapacitors Based on Carbon Nanoparticles/MnO₂ Nanorods Hybrid Structure. *ACS Nano* **6**, 656–661 (2011).
33. Zhang, X. *et al.* Solid-state flexible polyaniline/silver cellulose nanofibrils aerogel supercapacitors. *J Power Sources* **246**, 283–289 (2014).
34. Ranjusha, R. *et al.* Ultra fine MnO₂ nanowire based high performance thin film rechargeable electrodes: Effect of surface morphology, electrolytes and concentrations. *J Mater Chem* **22**, 20465 (2012).
35. Li, W. *et al.* MnO₂ ultralong nanowires with better electrical conductivity and enhanced supercapacitor performances. *J Mater Chem* **22**, 14864 (2012).
36. Cui, Y., Liu, Z.-H., Wang, M. & Ooi, K. New Approach to the Delamination of Layered Manganese Oxide. *Chem Lett* **35**, 740–741 (2006).
37. Liu, Z. *et al.* Synthesis and Delamination of Layered Manganese Oxide Nanobelts. *Chemistry of Materials* **19**, 6504–6512 (2007).
38. Wang, X. & Li, Y. Synthesis and Formation Mechanism of Manganese Dioxide Nanowires/Nanorods. *Chem. - Eur. J.* **9**, 300–306 (2003).
39. Sinha, A. K., Pradhan, M. & Pal, T. Morphological Evolution of Two-Dimensional MnO₂ Nanosheets and Their Shape Transformation to One-Dimensional Ultralong MnO₂ Nanowires for Robust Catalytic Activity. *J. Phys. Chem.C* **117**, 23976–23986 (2013).
40. Ren, L. *et al.* Adsorption–template preparation of polyanilines with different morphologies and their capacitance. *Electrochim Acta* **145**, 99–108 (2014).
41. Han, G. *et al.* MnO₂ nanorods intercalating graphene oxide/polyaniline ternary composites for robust high-performance supercapacitors. *Sci. Rep.* **4**, 4824 (2014).
42. Xu, M.-W. *et al.* Novel mesoporous MnO₂ for high-rate electrochemical capacitive energy storage. *Electrochim Acta* **55**, 5117–5122 (2010).
43. Huang, M. *et al.* Layered manganese oxides-decorated and nickel foam-supported carbon nanotubes as advanced binder-free supercapacitor electrodes. *J Power Sources* **269**, 760–767 (2014).
44. Yuan, C., Gao, B., Su, L. & Zhang, X. Interface synthesis of mesoporous MnO₂ and its electrochemical capacitive behaviors. *J. Colloid Interface Sci.* **322**, 545–550 (2008).
45. Yu, P. *et al.* Shape-Controlled Synthesis of 3D Hierarchical MnO₂ Nanostructures for Electrochemical Supercapacitors. *Cryst. Growth Des.* **9**, 528–533 (2008).
46. Lang, X., Hirata, A., Fujita, T. & Chen, M. Nanoporous metal/oxide hybrid electrodes for electrochemical supercapacitors. *Nat Nano* **6**, 232–236 (2011).
47. Kundu, M. & Liu, L. Direct growth of mesoporous MnO₂ nanosheet arrays on nickel foam current collectors for high-performance pseudocapacitors. *J Power Sources* **243**, 676–681 (2013).
48. Pech, D. *et al.* Ultrahigh-power micrometre-sized supercapacitors based on onion-like carbon. *Nat Nano* **5**, 651–654 (2010).
49. Luan, F. *et al.* High energy density asymmetric supercapacitors with a nickel oxide nanoflake cathode and a 3D reduced graphene oxide anode. *Nanoscale* **5**, 7984–7990 (2013).
50. Wang, G. *et al.* Solid-state supercapacitor based on activated carbon cloths exhibits excellent rate capability. *Adv Mater* **26**, 2676–2682, 2615 (2014).
51. Wang, Q. *et al.* NiCo₂O₄ nanowire arrays supported on Ni foam for high-performance flexible all-solid-state supercapacitors. *J. Mater. Chem. A* **1**, 2468 (2013).
52. Yang, P. & Mai, W. Flexible solid-state electrochemical supercapacitors. *Nano Energy* **8**, 274–290 (2014).

Acknowledgements

We gratefully acknowledge the financial support from the National Natural Science Foundation of China (21306026), Natural Science Foundation of Guangdong Province (S2012010009680), the Scientific Project of Guangdong Province (2014A010106030), the Foundation of Higher Education of Guangdong Province (2013CXZDA016), and Foundation for Distinguished Young Talents in Higher Education of Guangdong (2013LYM0024), and thank the Renewable Bioproduct Institute at Georgia Tech for general support.

Author Contributions

J.L.Z. and Y.L.D. designed the experiments, analyzed the data and wrote the manuscript. W.L. helped to carry out the electrochemical measurements of SSCs devices. X.D.Z. did SEM analysis. W.M. carried out TEM analysis. X.D. and Z.Z. provided the Ni foam. L.Y. and Y.L.D. gave revision of the manuscript. All authors have given approval to the final version of the manuscript.

Additional Information

Supplementary information accompanies this paper at <http://www.nature.com/srep>

Competing financial interests: The authors declare no competing financial interests.

How to cite this article: Zhou, J. *et al.* High Performance All-solid Supercapacitors Based on the Network of Ultralong Manganese dioxide/Polyaniline Coaxial Nanowires. *Sci. Rep.* **5**, 17858; doi: 10.1038/srep17858 (2015).



This work is licensed under a Creative Commons Attribution 4.0 International License. The images or other third party material in this article are included in the article's Creative Commons license, unless indicated otherwise in the credit line; if the material is not included under the Creative Commons license, users will need to obtain permission from the license holder to reproduce the material. To view a copy of this license, visit <http://creativecommons.org/licenses/by/4.0/>